Food Chemistry 365 (2021) 130461

Contents lists available at ScienceDirect

Food Chemistry

journal homepage: www.elsevier.com/locate/foodchem

Biosynthesis of α-solanine and α-chaconine in potato leaves (*Solanum tuberosum* L.) – A $^{13}CO_2$ study

Sebastian Baur [a], Oliver Frank [a], Hans Hausladen [c,e], Ralph Hückelhoven [c], Thomas Hofmann [a], Wolfgang Eisenreich [b,*], Corinna Dawid [a,d,*]

[a] Chair of Food Chemistry and Molecular Sensory Science, Technische Universität München, Lise-Meitner-Straße 34, 85354 Freising, Germany
[b] Bavarian NMR Center – Structural Membrane Biochemistry, Department of Chemistry, Technische Universität München, 85748 Garching, Germany
[c] Chair of Phytopathology, TUM School of Life Sciences, Technische Universität München, Emil-Ramann-Straße 2, 85354 Freising, Germany
[d] Bavarian Center for Biomolecular Mass Spectrometry, Technical University of Munich, Gregor-Mendel-Straße 4, 85354 Freising, Germany
[e] Plant Technology Center, TUM School of Life Sciences, Technische Universität München, Dürnast 4, 85354 Freising, Germany

ARTICLE INFO

Keywords:
Solanum tuberosum L.
Potato
Steroidal glycoalkaloids, α-solanine
α-Chaconine
Isotopologue profiling
$^{13}CO_2$

ABSTRACT

α-Solanine and α-chaconine are the major glycoalkaloids (SGAs) in potatoes, but up to now the biosynthesis of these saponins is not fully understood. *In planta* $^{13}CO_2$ labeling experiments monitored by nuclear magnetic resonance spectroscopy (NMR) and high-resolution mass spectrometry (HRMS) unraveled the SGA biosynthetic pathways from CO_2 photosynthates *via* early precursors to the SGAs. After a pulse of ~ 700 ppm $^{13}CO_2$ for four hours, followed by a chase period for seven days, specific ^{13}C-distributions were detected in SGAs from the leaves of the labeled plant. NMR analysis determined the positional ^{13}C-enrichments in α-solanine and α-chaconine characterized by $^{13}C_2$–pairs in their aglycones. These patterns were in perfect agreement with a mevalonate-dependent biosynthesis of the isopentenyl diphosphate and dimethylallyl diphosphate precursors. The ^{13}C-distributions also suggested cyclization of the 2,3-oxidosqualene precursor into the solanidine aglycone backbone involving a non–stereoselective hydroxylation step of the sterol a mixture of 25*S*-/25*R*-epimers of the SGAs.

1. Introduction

In terms of a harvest volume with 377 million tons per year (2016), potato (*Solanum tuberosum* L.) is one of the four most important food crops in the world, along with maize, wheat and rice (FAO, 2018). In addition to the nutritionally relevant metabolites, like carbohydrates and vitamins, such as vitamin C or B6, potatoes also contain biologically active secondary metabolites, such as glycoalkaloids. The two major glycoalkaloids of domesticated potatoes are α-solanine and α-chaconine, representing 95% of the total SGA content (Friedman & Levin, 2016). Both SGAs consist of a carbohydrate side chain (solatriose for α-solanine and chacotriose for α-chaconine), linked to C-3 of the steroidal C_{27} aglycone solanidine (Friedman, 2006) (see Fig. 1).

Besides the protective activity of glycoalkaloids against various pathogens and insects, they also have beneficial as well as harmful effects on humans (Friedman & Levin, 2016; Friedman, 2006). In low amounts, SGAs show an anticancerogenic potential against different cancer cell lines, for example human colon (HT29) and liver (HepG2) cancer cells (Friedman, Lee, Kim, Lee, & Kozukue, 2005; Lee et al., 2004). In contrast to their beneficial effects, higher doses of SGAs possess toxic effects to humans and can cause poisoning symptoms like vomiting or diarrhea (BfR, 2018).

Despite of the toxicological relevance of α-solanine and α-chaconine, the biosynthesis of the two major potato saponins is not completely understood (Cárdenas et al., 2015; Heftmann, 1983; Navarre, Shakya, & Hellmann, 2016). Isopentenyl diphosphate (IPP) and dimethylallyl diphosphate (DMAPP) are among the early precursors of the steroidal moiety. These C_5 units can be formed in plants *via* the classical mevalonate pathway in the cytosolic compartment or the more recently discovered MEP route (methylerythritol phosphate pathway) in the plastids (Bach, 1995; Eisenreich, Bacher, Arigoni, & Rohdich, 2004; Heftmann, 1983; KUZUYAMA & SETO, 2012; Lichtenthaler, Schwender, Disch, & Rohmer, 1997). In the case of SGAs, Guseva et al. already reported in the 60ties that both acetate and mevalonate are used for the

* Corresponding authors at: Chair of Food Chemistry and Molecukar Sensory Science, Technische Universität München, Lise-Meitner-Str. 34, 85354 Freising, Germany (C. Dawid) and Bavariam NMR Center - Structural Membrane Biochemistry, Department of Chemistry, Technische Universität München, 85748 Garching, Germany (W. Eisenreich).
E-mail addresses: wolfgang.eisenreich@mytum.de (W. Eisenreich), corinna.dawid@tum.de (C. Dawid).

https://doi.org/10.1016/j.foodchem.2021.130461
Received 15 January 2021; Received in revised form 2 May 2021; Accepted 23 June 2021
Available online 25 June 2021

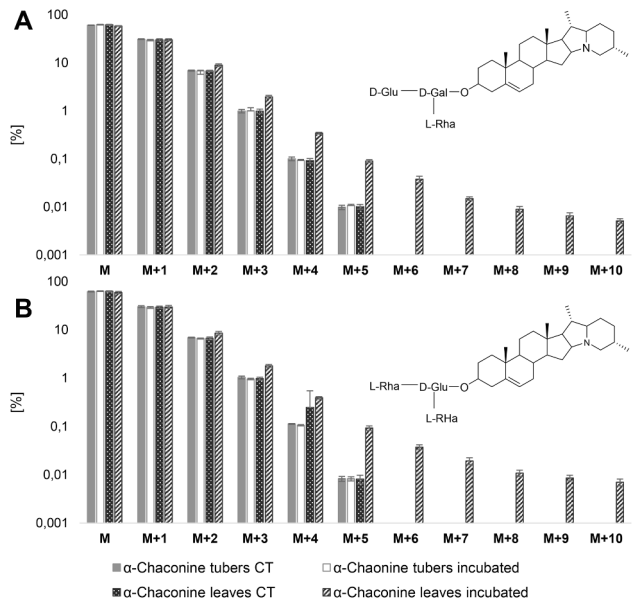

Fig. 1. Isotopomer distribution of α-solanine (A) and α-chaconine (B) in incubated and control potato tubers and leaves, based on detector count ratios of M + X (X = 1–10) over sum of all detector counts in percent. M represents $[M + H]^+$, while M + 1 to M + 10 is indicating isotopes with one up to ten ^{13}C atoms. Error bars indicate the standard deviation of two work-up replicates, which were measured three times.

biosynthesis of α-solanine and α-chaconine in potato leaves, seeds and sprouts (Guseva & Borokhima, 1960; Guseva, Paseshnichenko, & Borikhina, 1961; Kozukue, Tsuchida, & Friedman, 2001). Feeding experiments using radiotracers confirmed the role of mevalonate in SGA biosynthesis (Heftmann, 1983; Kozukue et al., 2001). However, the MEP route could not be excluded as a (minor) secondary SGA pathway due to the potential exchange of IPP and DMAPP precursors between the compartments in plants (Hampel, Mosandl, & Wüst, 2005; Laule et al., 2003; Schramek et al., 2010).

In the next step of SGA biosynthesis, two IPP and one DMAPP unit condensate to farnesyl pyrophosphate (C_{15}), followed by a tail-to-tail condensation of two C_{15} units to squalene (C_{30}) (Beeler, Anderson, & Porter, 1963; Heftmann, 1983). Squalene (C_{30}) is oxidized to 2,3-oxidosqualene (C_{30}) and converted into a C_{27} precursor *via* lanosterol (C_{30}) or cycloartenol (C_{30}), respectively (Cárdenas et al., 2015; Heftmann, 1983; Nes, 2011; Suzuki & Muranaka, 2007). Petersson et al. (2013) could identify cholesterol as a precursor of α-solanine and α-chaconine, using deuterium labeling experiments (Petersson et al., 2013). For the late steps of SGA biosynthesis, it is assumed that the C_{27} precursor (e.g. cholesterol) is hydroxylated at position C-22, followed by hydroxylation of the pro-*R* methyl position C-26 and C-16 (see also below) (Nakayasu et al., 2017; Umemoto et al., 2016). Then, the hydroxy function at position C-26 seems to be oxidized to the aldehyde intermediate, followed by a transamination step (Mikako, 1976; Ohyama, Okawa, Moriuchi, & Fujimoto, 2013). It is assumed that amino acids, like L-arginine, serve as a nitrogen source for this transamination (Mikako, 1976). Based on findings of naturally occurring metabolites in *Veratrum grandiflorum,* it was proposed that the F-ring of solanidine (C_{27}) is formed first *via* etioline (C_{27}) and 25*S*-teinemine (C_{27}), followed by dehydroxylation and ring closure at position C-16 (Heftmann, 1983; Mikako, 1976) finally leading to 25*S*-solanidine. Glycosylation of 25*S*-solanidine is then catalyzed by solanidine glycosyltransferases affording α-solanine and α-chaconine (Bergenstråhle, Tillberg, & Jonsson, 1992; Cárdenas et al., 2015; McCue et al., 2006).

In the present study, an *in planta* labeling strategy based on $^{13}CO_2$ (Eisenreich & Bacher, 2007) was exploited to reveal the biosynthetic pathway of SGAs in potato under *quasi*-physiological conditions. It turned out that, in combination with sophisticated NMR experiments, this strategy allowed to identify the early precursors, but also hitherto unknown steps in the cyclization of SGAs, notably in a single labelling experiment.

2. Material and Methods

2.1. Chemicals

$^{13}CO_2$ (99% ^{13}C-content), methanol d_4 and pyridine d_5 were obtained from Sigma-Aldrich (Steinheim, Germany). Methanol and acetonitrile used for the extraction and fractionation were purchased from Fisher Scientific U.K. Limited (Loughborough, United Kingdom). LC-MS-grade acetonitrile was purchased from Honeywell (Seelze, Germany). Ultrapure water for HPLC separation and mass spectrometry was purified using a Milli-Q-Water Advantage A 10 water system (Millipore, Molsheim, France). Potassium dihydrogen phosphate, used as buffered elution solvent for preparative HPLC, was obtained from Merck (Darmstadt, Germany), and α-solanine and α-chaconine were obtained from Phytolab (Vestenbergsgreuth, Germany).

2.2. Plants and $^{13}CO_2$ experiment

Two potato plants *Solanum tuberosum* L. 'Maxilla', one for the $^{13}CO_2$-labeling experiment, the other one as a control, were grown for four weeks under standardized conditions in a greenhouse (Dürnast, Freising, Germany). The labeling experiment was performed in a $^{13}CO_2$ incubation chamber according to (Eisenreich, Huber, Kutzner, & Knispel, 2013) (cf. Fig. S1, Supplementary Information). The potato plant was kept in the light under an atmosphere containing 600–800 ppm $^{13}CO_2$ for 4 h. To generate under these conditions fully labeled photosynthates, such as triose and pentose phosphates, $^{13}CO_2$ had to be constantly added while also constantly absorbing a fraction of CO_2 from the chamber to maintain the level of $^{12}CO_2$ (released by respiration) at < 100 ppm. During this period, the plant consumed about 500 mL of $^{13}CO_2$. After this pulse period, the plant was left for 7 days under standardized conditions in the greenhouse. The control plant was grown under natural circumstances in the greenhouse for the whole experimental period. Both plants were harvested by hand, tubers were washed and both plant materials (leaves and tubers) were directly prepared for high resolution mass spectrometry (HRMS) screening, to figure out, if this rather short $^{13}CO_2$–pulse period was enough to generate detectable ^{13}C-enrichments in the SGAs, and purification of SGAs for nuclear magnetic resonance spectroscopy (NMR).

2.3. HRMS screening of potato leaves and tubers

Leaves and tubers from both plants (supplied with $^{13}CO_2$ and control) were frozen in liquid nitrogen and ground in a laboratory blender (Grindomix GM300, Retsch, Haan, Germany), at 4000 U/min for 60 s. An amount of 3–5 g of the ground plant material was weighed in a bead beater tube (CK28, 15 mL, Bertin Technologies, Montigny-le-Bretonneux, France) and 5 mL of a mixture of MeOH/H_2O (7:3, v/v) was added. The samples were homogenized in a bead beater (Precellys Evolution, Bertin Technologies), supplied with a Cryolys cooling module (Bertin Technologies, cooled with liquid nitrogen), 3 times each, with 15 s breaks in between, at a speed of 6000 rpm. After centrifugation (5 min, 4000 rpm, RT), using an Eppendorf Centrifuge (5810R, Eppendorf, Hamburg, Germany), the clear supernatant (4 mL) was removed and the residue was extracted two more times with a mixture of MeOH/H_2O (7:3, v/v). The extracts were combined, freed from solvent and freeze dried. For MS analysis, the freeze-dried extracts were dissolved in MeOH/H_2O (7:3, v/v), resulting in a final concentration of 2 mg/mL. After membrane filtration (Minisart RC, Hydrophilic, 45 μm, Sartorius AG, Göttingen, Germany), the extracts were used for UPLC-HRMS analysis. α-Solanine and α-chaconine were identified in the extracts by

comparing the retention time, exact mass, fragmentation pattern and collision cross section (CCS) value with commercially available reference substances. Based on the ratio of the respective detector counts of each detected isotope over the detector counts of all detected isotopes, the relative isotopomer distribution (in percent) was determined.

2.4. Ultra-performance liquid chromatography/time-of-Flight mass spectrometry (UPLC/TOF-MS)

High resolution mass spectra were acquired of aliquots (2 μL) of the extracts, fractions and reference compounds, each dissolved in MeOH/H_2O (7:3, v/v). Data acquisition was done using a Waters Vion HDMS mass spectrometer (Waters, Manchester, UK) coupled to an Acquity i-class UPLC system (Waters, Milford, USA) equipped with a BEH C18 column (2 × 150 mm, 1.7 μm, Waters, Milford, USA) consisting of a binary solvent manager, sample manager and column oven. The chromatography was performed with a flow rate of 0.4 mL/min at 45 °C, using formic acid (0.1%) in water and formic acid (0.1%) in acetonitrile as solvents A and B and with the following gradient: starting with 5% B, increasing to 20% B in 2 min, increasing to 30% B in 7 min, increasing to 50% B in 1 min, holding at 50% B for 0.3 min isocratically, increasing to 100% B in 2.2 min, holding for 1 min isocratically, decreasing in 0.5 min to 5% B, and holding for 1 min isocratically. The MS system was operated in the ESI^+ sensitive mode, using the following conditions: 0.2 s scan time, 0.5 kV capillary voltage, 120 °C source temperature, 500 °C desolvation temperature, 50 L/h cone gas flow and 900 L/h desolvation gas, 6 eV low collision energy, 70–90 eV high collision energy. The system was operated, and the data was evaluated using UNIFI 1.8 (Waters, Milford, USA). For lock mass correction, leucine enkephaline (Tyr-Gly-Gly-Phe-Leu, *m/z* 556.2766, $[M + H]^+$) in a solution (50 pg/μL) of ACN/0.1% formic acid (1/1, v/v) was infused every 0.5 min with a scan time of 0.2 s. The MS system was calibrated between 50 and 1200 Da using a Major mix solution (Waters, Milford, USA).

2.5. Sequential solvent extraction

The upper part of the potato plant (stems and leaves; 250 g) was frozen in liquid nitrogen, milled in a knife mill (GM 300, Retsch, Haan, Germany) at 4000 rpm for 1 min and then extracted 3 times with ethylacetate (900 mL) by stirring for 20 min at room temperature. The sample was filtered using a suction filter, the filtrates were combined, and the solvent was removed under reduced pressure using a rotary evaporator (40 °C, 180 mbar). After lyophilization, the ethylacetate fraction (A) was obtained. The solid residue was extracted 3 times with a mixture of MeOH/H_2O (7/3, v/v, 900 mL) by stirring for 20 min at room temperature. Subsequently, the suspension was filtered and the filtrates were combined. The MeOH/H_2O fraction (B) was gained, after removing the solvent under reduced pressure (40 °C, 180 mbar), followed by a lyophilization step. The solid residue was extracted 3 times with water (900 mL) by stirring for 20 min at room temperature each. Next, the sample was filtered using a suction filter and each filtrate was combined. The extract was freeze dried to obtain fraction C. The extracts were stored at −20 °C until used for further fractionation. Using high resolution MS screening, fraction B could be identified as the glycoalkaloid-rich fraction.

2.6. Solid phase extraction (SPE) of fraction B

An aliquot of fraction B (0.8 g) was suspended in water (60 mL) and applied on a preconditioned Chromabond C18 ec cartridge (70 mL; 10 g, Macherey-Nagel, Düren, Germany). The stationary phase was conditioned by using methanol (60 mL) followed by a mixture of MeOH/H_2O (7/3, v/v, 60 mL) and water (60 mL). The sample was eluted stepwise, starting with water (100%, 60 mL) by increasing the MeOH content by steps of 10% up to methanol (100%, 60 mL), giving the fractions B-I (100/0, 60 mL), B-II (90/10, 60 mL), B-III (80/20, 60 mL), B-IV (70/30, 60 mL), B-V (60/40, 60 mL), B-VI (50/50, 60 mL), B-VII (40/60, 60 mL), B-VIII (30/70, 60 mL), B-IX (20/80, 60 mL), B-X (10/90, 60 mL) and B-XI (0/100, 60 mL). After the solvent was removed using vacuum evaporation (40 °C), the fractions were freeze dried and stored at −20 °C till further analysis. HRMS screening could identify the fractions B-VIII–B-XI as the glycoalkaloid rich fractions.

2.7. Preparative HPLC-Fractionation

Isolation of α-solanine and α-chaconine was performed on a preparative HPLC system (Jasco, Pfungstadt, Germany), using a Nucleodur C18 Pyramid column (250 × 21 mm, 5 μm, Macherey-Nagel, Düren, Germany) with a flow rate of 20 mL/min. The chromatographic separation was performed using an aqueous buffer solution (0.01 M KH_2PO_4, pH 0.8, solvent A) and acetonitrile (solvent B) with the following gradient: starting with 30% B, holding 30% B for 2 min isocratically, increasing in 38 min to 62% B, holding 62% B for 3 min, decreasing to 30% B in 2 min, holding 30% B for 5 min isocratically. The effluent was monitored at 202 nm, fractions B-VIII, B-IX and B-X resulted in 14, 9 and 5 subfractions, namely B-VIII-1–14, B-IX-1–9 and B-X-1–5. The separation was repeated about 50 times and corresponding fractions were combined. The fractions were freed from solvent by vacuum evaporation at 40 °C and lyophilized. The buffer was removed using a preconditioned Chromabond C18 ec cartridge (6 mL, 1 g, Macherey Nagel, Düren, Germany). Cartridge conditioning was done using methanol (6 mL), MeOH/H_2O (7/3, v/v, 6 mL) and water (6 mL). Every fraction was dissolved in water (6 mL), applied on the SPE cartridge and washed twice with water (6 mL) to remove the buffer. The fractions were eluted with methanol (16 mL). An aliquot (100 μL) of each fraction was used for HRMS analysis in order to identify the glycoalkaloid containing fractions. In addition, the solvent of the buffer free fractions was removed under a stream of nitrogen at room temperature, followed by lyophilization of the fractions. The two molecules of interest, α-solanine and α-chaconine could be identified in the fractions B-VIII-6 (2.0 mg), B-IX-3 (9.4 mg), B-XI-3 (10.5 mg), B-IX-8 (7.3 mg) as well as B-X-4 (10.2 mg) and B-XI-4 (15.s0 mg) comparing HRMS data of the isolated metabolites with commercially available reference substances. Fractions containing α-solanine and α-chaconine were combined and applied to NMR analysis. For structural identification of both SGAs, we compared the isolated metabolites with commercially available references by their exact masses, fragmentation patterns, retention times, CCS values and ^1H NMR data (cf. Figs. S5 and S6, Supporting Information). An overview of the isolation procedure can be found in the Supporting Information (cf. Fig. S4).

2.8. NMR spectroscopy of glycoalkaloids

α-Solanine (22 mg) and α-chaconine (32 mg) were dissolved in pyridine-d_5 (600 μL) mixed with 5 drops of methanol-d_4. ^{13}C NMR spectra were measured with a Bruker Avance-III 500 MHz spectrometer equipped with a cryo probe (5 mm CPQNP, $^1H/^{13}C/^{31}P/\ ^{19}F/^{29}Si$; Z-gradient). ^1H NMR spectra were registered with an Avance-III 500 MHz system and an inverse probe head (5 mm SEI, $^1H/^{13}C$; Z-gradient). The temperature was 300 K. Data processing and analysis was done with TOPSPIN 3.2 or MestreNova. The one-dimensional ^{13}C NMR spectrum as well as COSY, TOCSY, HSQC, HMBC, INADEQUATE and 1,1-ADEQUATE spectra were measured with standard Bruker parameter sets. In the INADEQUATE and 1,1-ADEQUATE experiments, the magnetization transfer between ^{13}C-atoms was optimized to a coupling constant of 45 Hz. For one-dimensional experiments, the FIDs were zero-filled and multiplied with a mild Gaussian function prior to Fourier transformation. The phase and the baseline of the spectra were manually corrected. Signals were manually integrated with appropriate controls of "empty" regions in the spectra. Integral values were verified by independent measurements using TOPSPIN or Mestre-Nova software. Absolute ^{13}C abundances were determined for selected positions *via* the

ratios of ^{13}C-coupled satellites in the global intensities of the respective ^{1}H NMR signals. Relative fractions of multiple-labeled isotopologues displaying ^{13}C^{13}C-couplings were quantified from the integral ratios of the satellite signals in the global intensities of the respective ^{13}C NMR signals.

3. Results

3.1. HRMS screening of $^{13}CO_2$ and untreated leaves

The $^{13}CO_2$ labelling experiment was performed according to protocols reported previously (Eisenreich et al., 2013; Schramek et al., 2014). The HRMS analysis of extracts from potato leaves and tubers confirmed the accumulation of ^{13}C-labeled α-solanine and α-chaconine in the leaves, but not in the tubers (Fig. 1). For example, the M + 5 fraction (i.e. molecules containing five ^{13}C-atoms) for SGAs in the labeled leaves was enriched by a factor of approximately 11 for α-chaconine and 9–fold for α-solanine, compared to the respective low ^{13}C-values for SGAs from leaves of the control caused by the natural (i.e. 1.1%) ^{13}C-abundance of ambient CO_2 in the greenhouse. In contrast to the control, isotopomers of M + 6 up to M + 10 could be only detected in the SGA of the incubated leaves. However, in the tubers no differences between the $^{13}CO_2$ sample and the control were detectable (Figs. S2 and S3, Supporting Information). This led to the assumption that there was no significant transport of labeled SGAs from the leaves to the tubers. The lack of transport of SGA upwardly had already been observed in potato tubers and roots (Friedman, 2006; Heftmann, 1983). Therefore, it is likely that SGA were also not transported from the upper part of the plant to the tubers. Based on this result, we subsequently isolated and purified mg amounts of SGAs, as described in Methods and Fig. S3, only from the leaves of the labeled plant.

3.2. NMR -analysis of the labeling patterns of α-solanine and α-chaconine

The NMR signals of the isolated SGAs were unequivocally assigned by two–dimensional ^{1}H^{1}H–, ^{1}H^{13}C-, and ^{13}C^{13}C-correlation experiments, such as COSY, HMBC, HSQC, INADEQUATE, and 1,1–ADEQUATE. Increased NMR-sensitivity could be achieved by the ^{13}C-enrichments of the labeled samples, which enabled the detection of ^{13}C^{13}C pairs by INADEQUATE and 1,1-ADEQUATE experiments. Moreover, the specific ^{13}C^{13}C-coupling constants detected for $^{13}C_2$-pairs in the ^{13}C NMR spectrum of the bio-labeled samples further solidified the assignments. In summary, the assignments were in agreement with literature data (Abouzid, Fawzy, Darweesh, & Orihara, 2008; Duggan, Dawid, Baur, & Hofmann, 2020). As a clear indication for multiple ^{13}C-labeling, the ^{13}C NMR signals of the ^{13}C-enriched SGAs showed satellites due to scalar couplings between adjacent ^{13}C-atoms (as examples, see Fig. 2). These satellites displayed narrow linewidths and distances in the range of 30–73 Hz due to $^{1}J_{CC}$ couplings (Table 1). We could not observe any long range couplings due to a third ^{13}C-atom connected to a $^{13}C_2$-moiety in a given molecule of the aglycone even after apodization with a more effective Gaussian function providing higher resolution. Notably, long-range couplings due to $^{13}C_3$-moities would serve as a valid indication for the contribution of the MEP pathway in the formation of the C5-precursor units *via* $^{13}C_3$-glyceraldehyde phosphate precursors (Schramek et al., 2010). On the basis of the missing long-range couplings, we conclude that the mevalonate route providing $^{13}C_2$-units *via* $^{13}C_2$-acetyl-CoA was the predominant pathway for the biosynthesis of the IPP and DMAPP precursors.

The relative intensities of the ^{13}C-satellite pairs in the overall NMR signal intensities of a carbon atom in the aglycone of α-solanine (12–42%) and α-chaconine (13–40%) (Table 1) exceeded the natural ^{13}C-^{13}C couplings of 1% by far. This shows that the experimental setting was successful in producing significant and specific data, as reflected by the similar coupling intensities for corresponding positions in α-solanine and α-chaconine (Table 1), also confirming the robustness of the analytical method.

To assign in detail the positional distributions of $^{13}C_2$-pairs in α-solanine and α-chaconine, INADEQUATE and 1,1-ADEQUATE experiments were most effective. INADEQUATE (incredible natural abundance double quantum transfer experiment) is a carbon-based NMR experiment, which uses $^{1}J_{CC}$ transfers to directly detect adjacent ^{13}C-^{13}C couplings. In contrast, the 1,1-ADQUATE (adequate double quantum transfer experiment) uses a $^{1}J_{CH}$ transfer followed by the evolution of the $^{1}J_{CC}$ couplings, to detect coupled ^{13}C-pairs (Reif, Köck, Kerssebaum, Kang, & Fenical, 1996).

Since α-solanine and α-chaconine consist of the same aglycone and virtually the same ^{13}C labeling pattern was observed for both SGAs, the data interpretation is now given in detail for α-solanine. However, the labeling pattern of α-chaconine served as a suitable control for the validity of our interpretation (cf. Figs. S7 and S8, Supplementary information).

On basis of the detected correlation in the INADEQUATE and ADEQUATE experiments, eleven $^{13}C_2$-isotopologues could be unequivocally identified in the aglycone of α-solanine. As already mentioned above, these $^{13}C_2$-units were confirmed by the specific coupling constants observed for the satellite pairs in the one-dimensional ^{13}C NMR spectrum (see Fig. 3 and Table 1).

In detail, [2,3-$^{13}C_2$]-, [5,6-$^{13}C_2$]-, [9,11-$^{13}C_2$]-, [10,19-$^{13}C_2$]-, [12,13-$^{13}C_2$]-, [13,18-$^{13}C_2$]-, [16,17-$^{13}C_2$]-, [20,21-$^{13}C_2$]-, [23,24-$^{13}C_2$]-, [25,27-$^{13}C_2$]-, and [25,26-$^{13}C_2$]-moieties could be determined. Except for the expected coupling between C-5 and C-6, all $^{13}C_2$-couplings were directly seen as correlations in the INADEQUATE and 1,1-ADEQUATE spectra. The coupling between C-5 and C-6 could be safely assumed

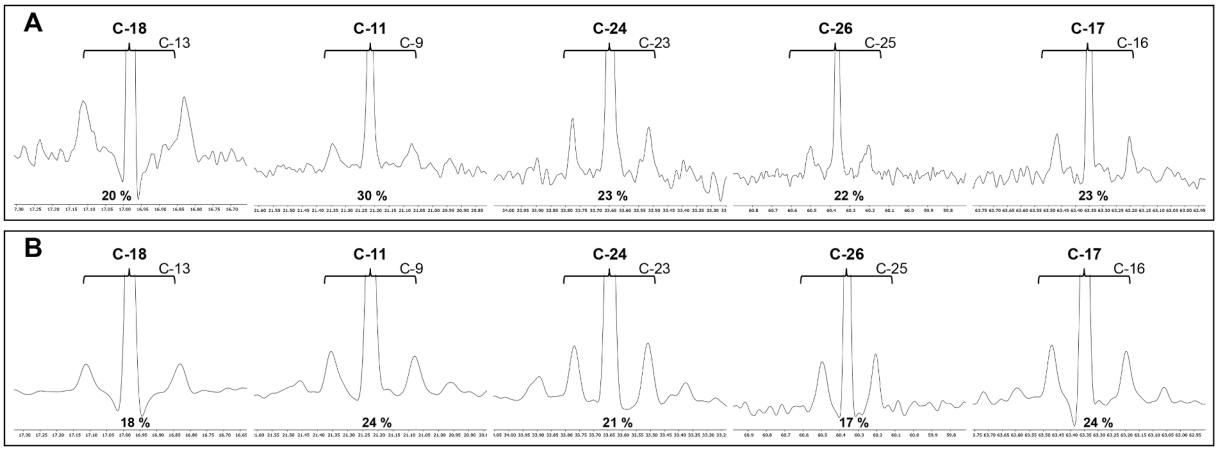

Fig. 2. Selection of ^{13}C satellite pairs of α-solanine (A) and α-chaconine (B), due to couplings of adjacent ^{13}C-atoms.

Table 1
Summary of the observed NMR data for the isolated α-solanine (sol.) and α-chaconine (chac.) from labelled potato leaves. The detailed ^{1}H- and ^{13}C-assignments can be found in Table S1, supporting information.

C-atom	^{13}C (δ) [ppm]		Relative signal intensity of ^{13}C^{13}C satellites [%]		J_{CC} [Hz]		Correlation with	Confirmed (+) with	
	Sol.	Chac.	Sol.	Chac.	Sol.	Chac.		ADEQUATE Sol./Chac.	INADEQUATE Sol./Chac.
1	37.63	37.60	n.d.	n.d.	n.d.	n.d.	–	–	–
2	30.22	30.22	18	13	37.0	37.6	3	+/+	+/+
3	77.61	78.19	22	26	37.6	38.5	2	+/+	+/+
4	38.87	39.04	n.d.	n.d.	n.d.	n.d.	–	–	–
5	140.92	140.83	20	23	71.8	72.6	6	–	–
6	121.97	122.03	19	32	71.5	72.6	5	–	–
7	32.47	32.44	n.d.	n.d.	n.d.	n.d.	–	–	–
8	31.98	31.96	n.d.	n.d.	n.d.	n.d.	–	–	–
9	50.53	50.54	20	15	35.1	34.1	11	+/+	+/+
10	37.18	37.16	20	15	35.2	35.0	19	–/–	+/+
11	21.22	21.23	30	24	34.4	35.0	9	+/+	+/+
12	40.10	40.08	34	31.0	36.1	35.7	13	+/+	+/+
13	40.55	40.54	20	21	29.7	36.0	12//18	–/–//–/–	+/+//+/+
14	57.79	57.76	12	17	35.3	32.2	–	–	–
15	31.59	31.59	21	20	37.0	31.3	–	–	–
16	69.32	69.30	25	19	36.6	34.7	17	+/+	+/+
17	63.35	63.35	23	24	32.9	34.7	16	+/+	+/+
18	16.98	16.98	20	18	35.7	35.0	13	+/+	+/+
19	19.45	19.45	35	32	29.7	33.2	10	+/+	+/+
20	36.94	36.94	24	20	36.7	37.6	21	+/+	+/+
21	18.54	18.49	35	37	35.2	36.0	20	+/+	+/+
22	74.80	74.79	n.e.	19	n.e.	37.6	–	–	–
23	29.62	29.63	34	19	34.2	33.2	24	+/+	+/+
24	33.65	33.64	23	21	33.1	32.2	23	+/+	+/+
25	31.36	31.35	24	19	35.2	35.7	26//27	+/–//+/–	+/+//+/+
26	60.36	60.36	22	17	37.7	37.6	25	+/+	+/+
27	19.69	19.69	36	36	30.4	33.2	25	+/+	+/+
1′	100.41	100.28	39	20	49.2	52.1	2′	+/+	+/+
2′	75.08	77.88	24	n.e.	40.9	n.e.	1′//3′	+/+//+/–	+/+//–/–
3′	84.91	77.84	n.d.	n.e.	n.d.	n.e.	–	–	–
4′	70.34	78.57	17	n.e.	39.5	n.e.	3′//5′	+/–//+/+	–/–//+/+
5′	76.44	76.89	18	4	42.0	42.0	4′//6′	+/–//+/+	+/–//+/+
6′	62.45	61.21	20	26	45.3	43.9	5′	+/+	+/+
1″	102.20	102.05	23	30	47.8	46.4	2″	+/+	+/+
2″	72.49	72.47	n.d.	n.e.	n.d.	n.e.	1″//3″	+/+//+/+	+/+//–/–
3″	72.69	72.69	n.d.	n.e.	n.d.	n.e.	n.d.	–	–
4″	74.04	73.99	18	18	40.2	43.9	5″	+/+	+/–
5″	69.48	69.55	17	13	43.0	42	4″/6″	–/+//+/+	+/–//+/+
6″	18.61	18.63	33	31	41.5	38.5	5″	+/+	+/+
1‴	105.86	102.87	42	28	49.2	47.4	2‴	+/+	+/+
2‴	74.85	72.44	20	n.e.	49.0	n.e.	1‴/3‴	+/+//+/+	+/+//–/–
3‴	78.36	72.59	n.e.	n.e.	n.d.	n.e.	–	–	–
4‴	71.42	73.79	18	27	40.9	43.8	3‴/5‴	+/–//–/+	–/–//+/–
5‴	78.31	70.41	n.e.	13	n.d.	41.0	4‴/6‴	+/+//+/+	+/–//+/+
6‴	62.45	18.46	20	40	45.3	38.1	5‴	+/+	+/+

*n.d. = not detectable **n.e. = not evaluable.

on basis of the specifically high coupling constant (72 Hz) between ^{13}C-5 and ^{13}C-6 in the one-dimensional spectrum. Due to this value, the missing correlation peak in the INADEQUATE and ADEQUATE spectra can be easily explained, since these experiments were optimized for ^{13}C-couplings with a coupling constant of 45 Hz, which was valid for most of the other carbon atoms in the SGAs.

The detected labeling pattern of the solanidine aglycone exactly matched the expected labeling pattern of the IPP and DMAPP precursors due to the mevalonate pathway and their subsequent assembly leading to 2,3-oxidosqualene (Fig. 4). Indeed, all 11 $^{13}C_2$-units predicted for a mevalonate origin (Fig. 4) were detected, but none of the $^{13}C_3$-isotopologues proposed for a MEP origin. Therefore, it can be concluded that the IPP and DMAPP precursors for the biosynthesis of α-solanine and α-chaconine were predominantly formed *via* the mevalonate pathway. Capitalizing on the sensitivity limits for NMR detection of hypothetical $^{13}C_3$-moieties, it can be estimated that contributions of potential IPP and DMAPP precursors derived from the MEP route were far below 5% (Schramek et al., 2014).

As another key result, [25,27-$^{13}C_2$]- and [25,26-$^{13}C_2$]-isotopologues were detected at similar abundances. This apparent randomization of a $^{13}C_2$-pair in ring F of the aglycone can be explained by a non-stereoselective hydroxylation of the terminal pro-*R* and pro-*S* methyl groups (C-26 and C-27) in the C_{27} sterol precursor (Fig. 5). The so far known biosynthesis of solanidine (Fig. 5, grey box) starts with a two-fold hydroxylation of cholesterol (leading to **1** and **2**) by cytochrome P450 *monooxygenases* (Umemoto et al., 2016). In the following, a hydroxylation at C-16 by a *2-oxoglutarate-dependent dioxygenase* leads to **3** (Nakayasu et al., 2017). Ohyama et al. (2013) suggested an involvement of an aldehyde intermediate (**4**) in the transamination mechanism, which leads to **5**. The following steps of solanidine biosynthesis (**5**–**8**) are not fully understood and here proposed according to Cárdenas et al. (2015), Heftmann (1983) and Keneko et al. (1976). This biosynthetic pathway results in the 25*S*-epimer of solanidine *via* 25*S*-tenemine with a $^{13}C_2$-pair between C-25 and C-26. However, this route does not explain the $^{13}C_2$-pair between C-25 and C-27 which was detected at a similar abundance as the C-25/C-26 ^{13}C-pair. An alternative pathway taking into account the C-25/C-27 ^{13}C-pair and leading to 25*R*-solanidine is shown in the blue box (Fig. 5). The major difference is the hydroxylation of 22-hydroxycholesterol at position C-27, which should lead to the formation of 25*R*-solanidine *via* 25*R*-tenemine. The final glycosylation

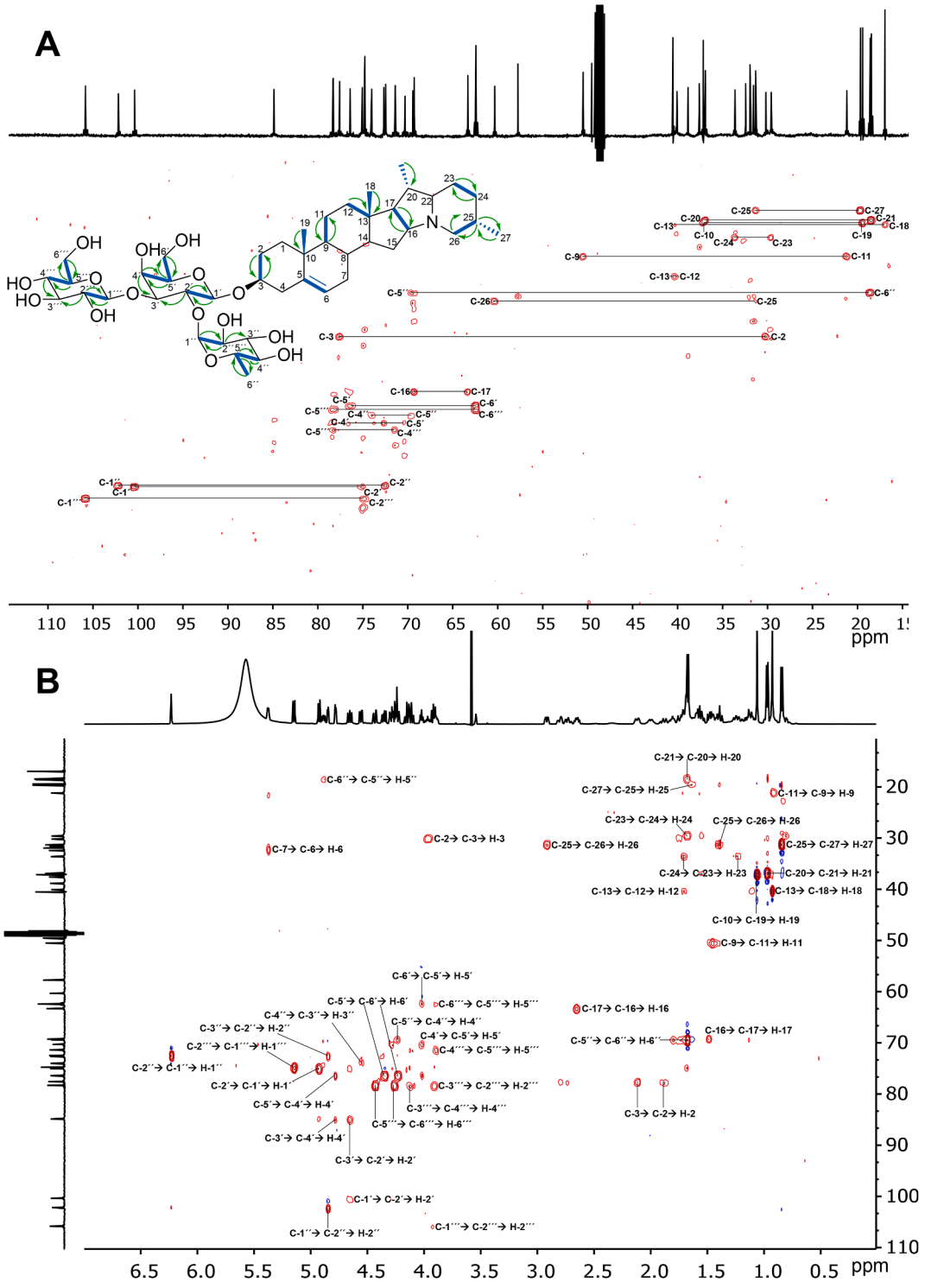

Fig. 3. Full INADEQUATE (A) and 1,1-ADEQUATE (B) spectrum of ^{13}C-labeled α-solanine from the $^{13}CO_2$ experiment. Couplings between adjacent ^{13}C-atoms are indicated with lines in the INADEQUATE (A) spectrum and highlighted with blue bold lines in the structure. 1,1-ADEQUATE (B) spectrum shows correlations between adjacent ^{13}C-atoms and its connected H-atom. The resulting couplings are indicated in the structure with green arrows. (For interpretation of the references to colour in this figure legend, the reader is referred to the web version of this article.)

of solanidine (**8**) to either α-solanine (**10**–**12**) or α-chaconine (**13**–**15**) is completed by different solanidine glycosyltransferases (SGTs) (Cárdenas et al., 2015).

So far, it has been assumed that only the 25*S*-epimer of α-solanine and α-chaconine are present in potatoes (Gaffield & Keeler, 1996; Ohyama et al., 2013). However, the 25*R*-epimer of solanidine has already been detected in the tubers of *Solanum vernei* (wild potato) and the leaves of a *Solanum tuberosum* clone, with *S. vernei* as progenitor (Van Gelder & Scheffer, 1991). The assumption of the 25*R*-epimer of solanidine is in accordance with the detected labelling patterns in our experiments suggestive to the partial formation of the 25*R*-epimers of α-solanine and α-chaconine, two 25*R*-solanidine glycosides, in potato leaves. Thus, the observed labeling pattern at position C-25–C-27 provides substantial evidence for a new alternative ring closure, involving

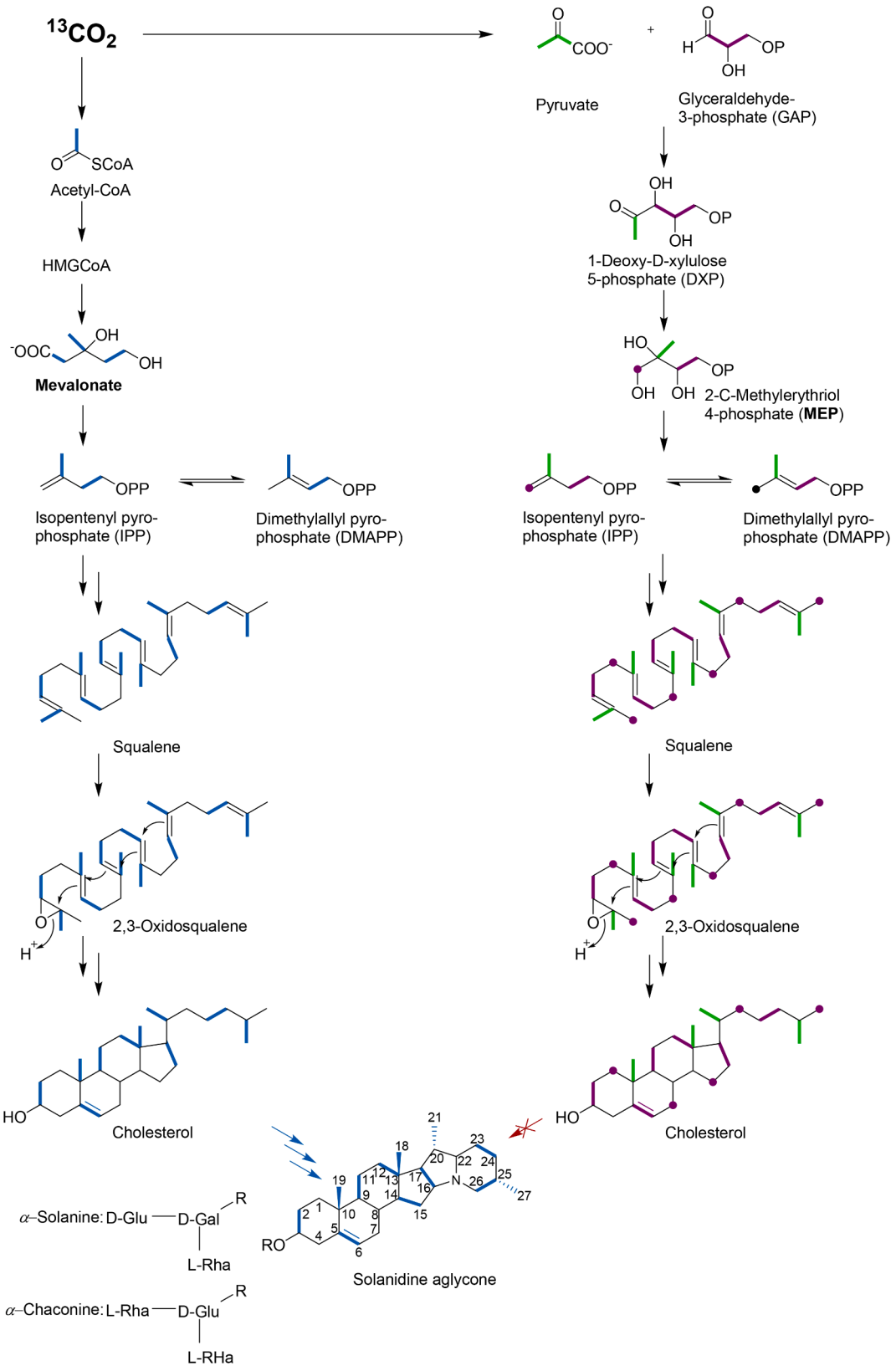

Fig. 4. Labeling patterns from $^{13}CO_2$ due to the biosynthesis of α-solanine and α-chaconine in potato leaves. Blue bold lines indicate the resulting $^{13}C_2$ units via mevalonate pathway, whereas purple and green bold lines indicate the expected ^{13}C-units and labeling patterns resulting from MEP route. Purple dots mark single labeled carbon atoms resulting from the separation of the C_3 unit (glyceraldehyde phosphate precursor). The biosynthesis was proposed according to Cárdenas et al. (2015), Heftmann (1983) and Nes (2011). The labeling pattern of the solanidine aglycone is observed in α-solanine and α-chaconine. The labeling patterns upstream of the saponins are predicted. (For interpretation of the references to colour in this figure legend, the reader is referred to the web version of this article.)

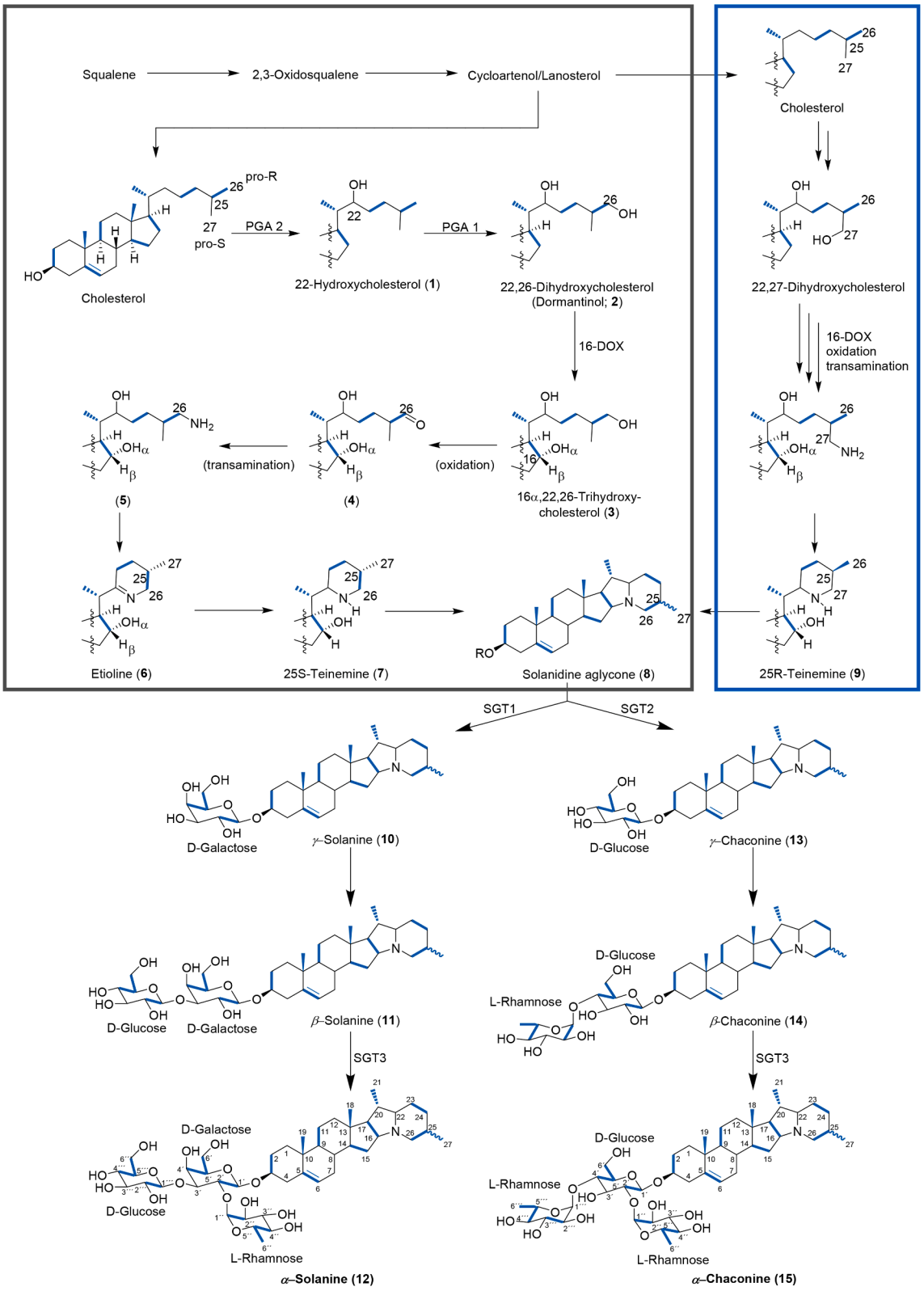

Fig. 5. Hypothetical pathways for the biosynthesis of 25*S*-solanidine aglycone (8) as shown in the grey box, according to Cárdenas et al. (2015), Heftmann (1983), Kaneko et al. (1976), Nakayasu et al. (2017), Ohyama et al. (2013), Umemoto et al. (2016). The new alternative biosynthesis of 25*R*-solanidine is shown in the blue box. The glycosylation of solanidine (8) to *α*-solanine (10–12) or *α*-chaconine (13–15) is displayed according to Cárdenas et al. (2015). The bonds indicated by bold lines in blue indicate the ^{13}C-patterns in the labeling experiment with $^{13}CO_2$. (For interpretation of the references to colour in this figure legend, the reader is referred to the web version of this article.)

hydroxylation of 22-hydroxycholesterol at position C-27, followed by formation of 25*R*-teinemine and 25*R*-solanidine. This result disproves with previous studies, in which the formation of solanidine *via* hydroxylation at the pro-*R* group was assumed, whereas a hydroxylation at the pro-*S* group resulted in solasodine (Ohyama et al., 2013).

Due to the signal overlaps in the ^{13}C NMR spectra of the sugar moieties in *α*-solanine and *α*-chaconine, not all couplings could be evaluated (see Table 1). Nevertheless, the NMR experiments allowed to assign the following $^{13}C_3$-isotopologues for both SGAs (see Fig. 3): [1′,2′,3′-$^{13}C_3$], [4′,5′,6′-$^{13}C_3$], [1‘‚2″,3″-$^{13}C_3$], [4″,5″,6″-$^{13}C_3$], [1‴,2‴,3‴-$^{13}C_3$], and [4‴,5‴,6‴-$^{13}C_3$]. These $^{13}C_3$-isotopologues are in perfect agreement with the formation of the sugars *via* $^{13}C_3$-3-phosphoglycerate units (Alberts, Johnson, & Lewis, 2002) as formed during the photosynthetic process of $^{13}CO_2$ fixation. This finding can be taken as another verification of the experimental approach. Unexpectedly, the relative fractions of ^{13}C-coupled isotopologues were significantly different for C-1′ (D-galactose, 39%), C-1″ (L-rhamnose, 23%) and C-1‴ (D-glucose, 42%) of *α*-solanine. For *α*-chaconine, on the other hand, the anomeric carbon atoms showed ^{13}C couplings of 20% for C-1′ (D-glucose), 30% for C-1″ (L-rhamnose) and 28% for C-1‴ (L-rhamnose). This variation is not understood, but it is tempting to speculate that these differences reflect a considerable high degree of dynamics in the glycosylation steps which could be different for *α*-chaconine and α-solanine biosynthesis.

4. Conclusion

This study further highlights the power of the $^{13}CO_2$ labeling technique to elucidate key processes in the biosynthesis of secondary metabolites as a corner stone for further studies of enzymes involved in the respective biosynthesis. Here, the labelling profiles of two complex steroidal glycoalkaloids from potato displayed highly distinct and specific ^{13}C-distributions. These patterns reflected the experimental setting in the $^{13}CO_2$ pulse chase experiment. As a logical consequence of the $^{13}CO_2$ pulse and chase period, a mixture of $^{13}C_2$-labelled acetyl-CoA and unlabeled acetyl-CoA served as the building units for the making of the solanidine aglycones finally resulting in the observed “mosaics” of carbon isotopologues that demonstrated the mevalonate origin of the IPP and DMAPP precursors, but also showed mechanisms during the downstream biosynthetic pathway such as regio- and stereospecific events in the cyclization process. Due to the experimental settings, these observations reflected more-or-less physiological conditions since CO_2 is the natural carbon source for plants. In sum, we were able to get a deeper inside into the biosynthesis pathway of SAGs in potato. We could show that a predominant fraction, if not all, of the IPP and DMAPP precursors for SGA biosynthesis is formed *via* the mevalonate pathway. This finding adds another example for the mevalonate origin of a steroidal product in plants. Since the mevalonate pathway is operative in the cytosolic compartment of a plant cell, in sharp contrast to the plastidic MEP pathway, it is plausible that the subsequent steps of SGA biosynthesis also proceed in the cytosolic compartment, most likely under contribution of cytochrome P450 monooxygenases at the cytosolic interface of endoplasmic reticulum. Furthermore, due to the label distribution in the C-25–C27 moiety of the aglycone, we could propose a non-stereoselective ring closure and therefore, an alternative F ring formation leading to 25*R*-solanidine epimers and therefore to 25*R*-*α*-solanine and 25*R*-*α*-chaconine. So far, only the predominant 25*S*-epimer of both SGAs was described in potatoes. It is very likely that the 25*R*-epimer was not detected, because of the high excess of the 25*S*-epimer over the 25*R*-epimer, combined with the limit of detection of the NMR experiments used for the analysis in the past. Additional studies will be necessary to investigate the detailed mechanism on the level of the enzymes, but also the bioactivities of the respective epimers, since epimers can have different biological properties, as shown for example for the polyketides (1*S*, 3*S*)-austrocortilutein and (1*R*, 3*R*)-austrocortilutein found in *Dermocybe splendida*. In that case (1*S*, 3*S*)-austrocortilutein has antibiotic activity, whereas (1*R*, 3*R*)-austrocortilutein shows no activity (Finefield, Sherman, & Robert, 2012).

CRediT authorship contribution statement

Sebastian Baur: Methodology, Formal analysis, Visualization, Investigation, Writing - original draft. **Oliver Frank:** Methodology, Writing - review & editing. **Hans Hausladen:** Resources, Writing - review & editing. **Ralph Hückelhoven:** Resources, Writing - review & editing. **Thomas Hofmann:** Resources, Supervision. **Wolfgang Eisenreich:** Methodology, Project administration, Funding acquisition, Writing - review & editing, Supervision. **Corinna Dawid:** Supervision, Project administration, Funding acquisition, Writing - review & editing.

Declaration of Competing Interest

The authors declare that they have no known competing financial interests or personal relationships that could have appeared to influence the work reported in this paper.

Acknowledgements

The authors are thankful for financial support from the Fonds der Chemischen Industrie, and the Leonhard-Lorenz foundation (No. 912/15). W.E. thanks the BMBF “Maßgeschneiderte Inhaltsstoffe 2” (ASPIRANT, grant number 031B0823D) and the Hans-Fischer-Gesellschaft (Munich, Germany) for financial support.

Appendix A. Supplementary data

Supplementary data to this article can be found online at https://doi.org/10.1016/j.foodchem.2021.130461.

References

Abouzid, S., Fawzy, N., Darweesh, N., & Orihara, Y. (2008). Steroidal glycoalkaloids from the berries of Solanum distichum. *Natural Product Research, 22*(2), 147–153.
Alberts B, Johnson A, Lewis J, et al. (2002). Chloroplasts and Photosynthesis. In B. Alberts (Ed.), Molecular biology of the cell (4th ed.). New York, NY: Garland Science.
Bach, T. J. (1995). Some new aspects of isoprenoid biosynthesis in plants–a review. *Lipids, 30*(3), 191–202.
Beeler, D. A., Anderson, D. G., & Porter, J. W. (1963). The biosynthesis of squalene from mevalonic acid-2-C14 and farnesyl pyrophosphate-4,8, 12–C14 by carrot and tomato enzymes. *Archives of Biochemistry and Biophysics, 102*(1), 26–32.
Bergenstråhle, A., Tillberg, E., & Jonsson, L. (1992). Characterization of UDP-glucose: Solanidine glucosyltransferase and UDP-galactose:Solanidine galactosyltransferase from potato tuber. *Plant Science, 84*(1), 35–44.
BfR (2018, April 23). Table potatoes should contain low levels of glycoalkaloids (solanine). Opinion No 010/2018 [Press release].
Cárdenas, P. D., Sonawane, P. D., Heinig, U., Bocobza, S. E., Burdman, S., & Aharoni, A. (2015). The bitter side of the nightshades: Genomics drives discovery in Solanaceae steroidal alkaloid metabolism. *Phytochemistry, 113*, 24–32.
Duggan, T., Dawid, C., Baur, S., & Hofmann, T. (2020). Characterization of bitter and astringent off-taste compounds in potato fibers. *Journal of Agricultural and Food Chemistry, 68*(41), 11524–11534. https://doi.org/10.1021/acs.jafc.0c04853.
Eisenreich, W., Bacher, A., Arigoni, D., & Rohdich, F. (2004). Biosynthesis of isoprenoids via the non-mevalonate pathway. *Cellular and Molecular Life Sciences : CMLS, 61*(12), 1401–1426.
Eisenreich, W., & Bacher, A. (2007). Advances of high-resolution NMR techniques in the structural and metabolic analysis of plant biochemistry. *Phytochemistry, 68*(22–24), 2799–2815. https://doi.org/10.1016/j.phytochem.2007.09.028.
Eisenreich W, Huber C, Kutzner E, Knispel N, & Schramek N (Eds.) (2013). Isotopologue Profiling – Toward a Better Understanding of Metabolic Pathways: The handbook of plant metabolomics. Kahl, Günter; Weckwerth, Wolfram. Molecular plant biology handbook series. Weinheim: Wiley-VCH Verlag GmbH.
FAO. (2018). *World food and agriculture: Statistical pocketbook 2018*. Rome: Food and Agriculture Organization of the United Nations.
Finefield, J. M., Sherman, D. H., Kreitman, M., & Williams, R. M. (2012). Enantiomere naturstoffe: Vorkommen und biogenese. *Angewandte Chemie, 124*(20), 4886–4920. https://doi.org/10.1002/ange.201107204.
Friedman, M. (2006). Potato glycoalkaloids and metabolites: Roles in the plant and in the diet. *Journal of Agricultural and Food Chemistry, 54*(23), 8655–8681.
Friedman, Mendel, Lee, Kap-Rang, Kim, Hyun-Jeong, Lee, In-Seon, & Kozukue, Nobuyuke (2005). Anticarcinogenic effects of glycoalkaloids from potatoes

against human cervical, liver, lymphoma, and stomach cancer cells. *Journal of Agricultural and Food Chemistry, 53*(15), 6162–6169.
Friedman, M., & Levin, C. E. (2016). Glycoalkaloids and calystegine alkaloids in potatoes. In *Advances in Potato Chemistry and Technology* (pp. 167–194). Elsevier.
Gaffield, William, & Keeler, Richard F. (1996). Induction of terata in hamsters by solanidane alkaloids derived from Solanum tuberosum. *Chemical Research in Toxicology, 9*(2), 426–433.
Guseva, A. R., Borokhima, M. G., & Paseshnichenko, V. (1960). Utilization of acetate for the biosynthesis of chaconine and solanine in potato sprouts. *Biokhimiia (Moscow, Russia), 25*, 282–284.
Guseva, A. R., Paseshnichenko, V. A., & Borikhina, M. G. (1961). Synthesis of radioactive mevalonic acid and its use for the study of the biosynthesis of the steroid glycoalkaloids of Solanum. *Biokhimiia (Moscow, Russia), 26*, 723–728.
Hampel, D., Mosandl, A., & Wüst, M. (2005). Biosynthesis of mono- and sesquiterpenes in carrot roots and leaves (Daucus carota L.): Metabolic cross talk of cytosolic mevalonate and plastidial methylerythritol phosphate pathways. *Phytochemistry, 66*(3), 305–311. https://doi.org/10.1016/j.phytochem.2004.12.010.
Heftmann, E. (1983). Biogenesis of steroids in solanaceae. *Phytochemistry, 22*(9), 1843–1860.
Kaneko, K., Tanaka, M. W., & Mitsuhashi, H. (1976). Origin of nitrogen in the biosynthesis of solanidine by Veratrum grandiflorum. *Phytochemistry, 15*(9), 1391–1393.
Kozukue, N., Tsuchida, H., & Friedman, M. (2001). Tracer studies on the incorporation of 2–14C-DL-mevalonate into chlorophylls a and b, alpha-chaconine, and alpha-solanine of potato sprouts. *Journal of Agricultural and Food Chemistry, 49*(1), 92–97.
Kuzuyama, T., & Seto, H. (2012). Two distinct pathways for essential metabolic precursors for isoprenoid biosynthesis. *Proceedings of the Japan Academy. Series B, Physical and Biological Sciences, 88*(3), 41–52.
Laule, O., Fürholz, A., Chang, H.-S., Zhu, T., Wang, X., Heifetz, P. B., & Lange, M. (2003). Crosstalk between cytosolic and plastidial pathways of isoprenoid biosynthesis in Arabidopsis thaliana. *Proceedings of the National Academy of Sciences of the United States of America, 100*(11), 6866–6871. https://doi.org/10.1073/pnas.1031755100.
Lee, Kap-Rang, Kozukue, Nobuyuki, Han, Jae-Sook, Park, Joon-Hong, Chang, Eun-young, Baek, Eun-Jung, et al. (2004). Glycoalkaloids and metabolites inhibit the growth of human colon (HT29) and liver (HepG2) cancer cells. *Journal of Agricultural and Food Chemistry, 52*(10), 2832–2839.
Lichtenthaler, H. K., Schwender, J., Disch, A., & Rohmer, M. (1997). Biosynthesis of isoprenoids in higher plant chloroplasts proceeds via a mevalonate-independent pathway. *FEBS Letters, 400*(3), 271–274. https://doi.org/10.1016/S0014-5793(96)01404-4.
McCue, Kent F., Allen, Paul V., Shepherd, Louise V. T., Blake, Alison, Whitworth, Jonathan, Malendia Maccree, M., et al. (2006). The primary in vivo steroidal alkaloid glucosyltransferase from potato. *Phytochemistry, 67*(15), 1590–1597.
Nakayasu, Masaru, Umemoto, Naoyuki, Ohyama, Kiyoshi, Fujimoto, Yoshinori, Lee, Hyoung Jae, Watanabe, Bunta, et al. (2017). A dioxygenase catalyzes steroid 16α-hydroxylation in steroidal glycoalkaloid biosynthesis. *Plant Physiology, 175*(1), 120–133.
Navarre, D. A., Shakya, R., & Hellmann, H. (2016). Vitamins, phytonutrients, and minerals in potato. In *Advances in Potato Chemistry and Technology* (pp. 117–166). Elsevier.
David Nes, W. (2011). Biosynthesis of cholesterol and other sterols. *Chemical Reviews, 111*(10), 6423–6451.
Ohyama, Kiyoshi, Okawa, Akiko, Moriuchi, Yuka, & Fujimoto, Yoshinori (2013). Biosynthesis of steroidal alkaloids in Solanaceae plants: Involvement of an aldehyde intermediate during C-26 amination. *Phytochemistry, 89*, 26–31.
Petersson, Erik V., Nahar, Nurun, Dahlin, Paul, Broberg, Anders, Tröger, Rikard, Dutta, Paresh C., et al. (2013). Conversion of exogenous cholesterol into glycoalkaloids in potato shoots, using two methods for sterol solubilisation. *PloS One, 8*(12), e82955. https://doi.org/10.1371/journal.pone.0082955.
Reif, B., Köck, M., Kerssebaum, R., Kang, H., Fenical, W., & Griesinger, C. (1996). ADEQUATE, a New Set of Experiments to Determine the Constitution of Small Molecules at Natural Abundance. *Journal of Magnetic Resonance, Series A, 118*(2), 282–285. https://doi.org/10.1006/jmra.1996.0038.
Schramek, N., Huber, C., Schmidt, S., Dvorski, S. E., Knispel, N., Ostrozhenkova, E., et al. (2014). Biosynthesis of ginsenosides in field-grown panax ginseng. *JSM Biotechnology & Biomedical Engineering, 2(1*, 1033.
Schramek, N., Wang, H., Römisch-Margl, W., Keil, B., Radykewicz, T., Winzenhörlein, B., et al. (2010). Artemisinin biosynthesis in growing plants of Artemisia annua. A 13CO2 study. *Phytochemistry, 71*(2–3), 179–187.
Suzuki, M., & Muranaka, T. (2007). Molecular genetics of plant sterol backbone synthesis. *Lipids, 42*(1), 47–54. https://doi.org/10.1007/s11745-006-1000-5.
Umemoto, Naoyuki, Nakayasu, Masaru, Ohyama, Kiyoshi, Yotsu-Yamashita, Mari, Mizutani, Masaharu, Seki, Hikaru, et al. (2016). Two cytochrome P450 monooxygenases catalyze early hydroxylation steps in the potato steroid glycoalkaloid biosynthetic pathway. *Plant Physiology, 171*(4), 2458–2467.
Van Gelder, W. M. J., & Scheffer, J. J. C. (1991). Transmission of steroidal glycoalkaloids from Solanum vernei to the cultivated potato. *Phytochemistry, 30*(1), 165–168. https://doi.org/10.1016/0031-9422(91)84118-C.